Inter-annual Variability of the Current System off the West Greenland Coast from a very high-resolution numerical model

Enter authors here: Ruijian Gou[1,2], Clark Pennelly[2] and Paul G. Myers

[1]Key Laboratory of Physical Oceanography and Frontiers Science Center for Deep Ocean Multispheres and Earth System, Ocean University of China, Qingdao, China

[2]Department of Earth and Atmospheric Sciences, University of Alberta, Edmonton, Alberta, Canada.

Corresponding author: Paul G. Myers (mailto:pmyers@ualberta.ca)

Key Points:

- The net freshwater transport of the WGC does not drop between Cape Desolation and Fylla Bank sections
- Along southwest Greenland, the shelf component weakens while the shelf break component strengthens, both by >0.1 m s^{-1} , over 2008-2018.
- The current system is buoyancy driven near southwest Greenland, with wind forcing more dominant in the north.

Abstract

Analyzing a high-resolution (1/60°) numerical model over 2008 to 2018, the inter-annual variability of the West Greenland Coastal Current (WGCC) on the shelf and West Greenland Current (WGC) at shelf break is presented. Both currents flow from Cape Farewell and extend to Davis Strait, with their model speeds and transports corresponding well with observations. The inter-annual variability of the WGCC and WGC near southwest Greenland are opposite, with the former declining while the latter strengthened, both by a speed change above 0.1 m/s. Both currents are predominantly buoyancy forced, but wind forcing becomes more dominant towards Davis Strait. The main exchanges from the two currents to interior occur between Cape Desolation and Fylla Bank, with net volume, freshwater, heat transport decreases of 1.4 Sv, 13 mSv, 36.7 TW. The freshwater transport of the WGC itself does not drop in between these sections, receiving freshwater from the WGCC to compensate for the losses to the basin interior. Thus, we see significant freshwater (83.1 mSv) and heat transports (70.7 TW) of the WGC remaining at Fylla Bank that reach the northern basin instead of being fluxed into the interior pof the Labrador Sea. This suggests that the exchange between the current system and the interior is more limited than previously thought, and most of the Greenland and Arctic melt reaches the northern Labrador Sea. Our results highlight the importance of resolving the WGCC and shelf processes.

Plain Language Summary

The West Greenland Coastal Current (WGCC) is a shelf current that carries the cold and fresh water from the Arctic and Greenland, and the West Greenland Current (WGC) is a shelf break current that carries the Arctic water at surface and warm, salty Atlantic water at depth. Their transports could have a significant impact on the stratification in the Labrador Sea. However, due

to the lack of observations and insufficient model resolution, their inter-annual variabilitiy is not understood yet. In this study, we present their inter-annual variability along the west Greenland coast, from a high-resolution numerical model from 2008 to 2018. Both currents flow from Cape Farewell north to Davis Strait. The variability of the WGCC and WGC near southwest Greenland are opposite, with the former declining while the latter strengthened. The currents are forced by both wind and buoyancy, with wind more important the further north. Between Cape Desolation and Fylla Bank is where the most offshore exchanges from the currents to the interior Labrador Sea occurs. Nevertheless, the exchanges are limited as the majority of the freshwater and heat flows to the north.

1 Introduction

1.1 West Greenalnd Current

The West Greenland Current (WGC; Figure 1) has a significant role in modulating the deep convection in the Labrador Sea (Li et al., 2021), where an important mode water – Labrador Sea Water (LSW), is produced. It is a strong current that is situated on the shelf break of west Greenland. It carries a significant amount of buoyant water, with low salinity water of Arctic origin at the surface, as well as the warm and salty Irminger water at intermediate depths (Myers et al., 2007; Fratatoni and Pickart, 2007; Pacini et al., 2021). These water masses are transported into the interior Labrador Sea either through offshore Ekman transport (e.g., Luo et al., 2016; Schulze-Chretien & Frajka-Williams, 2018) or eddies (e.g., Bracco et al., 2008; de Jong et al., 2014; Katsman et al., 2004). This lateral exchange offers a buoyancy flux to restratify the water column (Luo et al., 2016), thus affecting the deep convection. Therefore, the WGC's volume/freshwater transport can significantly modulate the density anomaly across the Labrador Sea (Zou et al., 2020) impacting convection, LSW formation and potentially the Atlantic Meridional Overturning Circulation (AMOC; Li et al., 2021).

In terms of the WGC transports, Myers et al. (2009) calculated a mean summer volume transport (relative to the 34.8 isohaline and 700 db) for 1984-2005 of 5.5 ± 3.9 Sv at the Cape Desolation section that decreases northward to 0.0 ± 0.3 Sv at the Sisimiut section , using the data from the Greenland Institute of Natural Resources (GINR) standard sections (Figure 2; Mortensen, 2018). The corresponding mean freshwater transports, referenced to a salinity of 34.8 are 54.4 ± 22.4 mSv at Cape Desolation section and 0.03 ± 5.4 mSv at Sisimiut section. Using multiple hydrography datasets for 1992-2008, Rykova et al. (2015) showed a mean volume transport (relative to the 3000 m isobath, 34.4 isohaline and 1000 db) of 1.8 ± 0.15 Sv and a mean freshwater transport of 60.1 ± 16 mSv (referenced to a salinity of 34.3) at the AR7W section. Besides those observational studies, a study using an eddy-permitting model showed that the mean northward components of the volume transport and freshwater transport referenced to a salinity of 34.8 for 1965-2002 across the Davis Strait are 1.2 Sv and 15.7 mSv respectively (Lique et al., 2009), despite the net transport at Davis Strait being southward (Curry et al., 2011, 2014). An eddy-rich modelling study revealed that the mean WGC volume transports for 2004-2013 at Maniitsoq and Sisimiut are ~0.8 Sv and ~0.7 Sv respectively, and the corresponding mean WGC heat transports referenced to 0°C are ~10 TW for each section (Myers et al., 2021). However, the transport comparison among the studies is difficult considering the different time periods and definitions for the currents.

1.2 West Greenalnd Coastal Current

As a part of the West Greenland Current system, the West Greenland Coastal Current (WGCC; Figure 1), a recently discovered shelf current (Lin et al., 2018), has recently received attention since it carries the coldest and freshest water in this region, the upper polar water (Pacini et al, 2020). It was found that the East Greenland Coastal Current (EGCC), located on the east Greenland shelf, keeps its identity rounding Cape Farewell (Lin et al., 2018; Pacini et al, 2020), becoming the WGCC. That said, the WGCC is distinguished from the EGCC as its boundary with the shelf break current is not as clear (Duryck et al., 2021; Gou et al., 2021). Furthermore, it has been suggested that their may be considerable exchange between the WGCC and the WGC near Cape Farewell (Lin et al., 2018; Gou et al., 2021).

The WGCC was first demonstrated in the analysis of a summer cruise survey data in 2014 (Lin et al., 2018). They showed that as it goes from Cape Farewell to Cape Desolation, its volume transport and freshwater transport decrease from 1.01 Sv to 0.42 Sv and from 49.50 mSv to 23.32 mSv, respectively (referenced to 34.8). Recently, its seasonality was studied by the sectional data from the Overturning in the Subpolar North Atlantic Program (OSNAP; Lozier et al., 2017) (Pacini et al., 2020) and combined in situ and satellite data (Majumder et al., 2021). Additionally, a recent high-resolution modelling study (Gou et al, 2021) has revealed very similar seasonal features as these observations showed, such as the seasonal transport cycles.

Nevertheless, the inter-annual variability of the WGCC and WGC remain largely unknown, considering the short time-span (2014-2018) of the OSNAP data and the mainly summertime occupations of the other sections. Additionally, the fate of the WGCC north of Cape Desolation is an open question. Thus our use of a very high-resolution numerical model provides an useful tool for studying the behavior of the WGC/WGCC system along the west Greenland coast, including the system's inter-annual variability. Given its ability to resolve the Rossby radius and many mesoscale features with a resolution reaching 800 m, the model is able to represent realistic behavior on the shelf (e.g. Pennelly and Myers, 2021, Gou et al., 2021), as well as the offshore exchange into the Labrador Sea (e.g. Pennelly and Myers, 2021). Thus, we use a decade of output of our model to study the inter-annual variability of the WGCC and WGC, analyzing the currents and their speed, transports and forcings, as well as the exchange into the Labrador Sea.

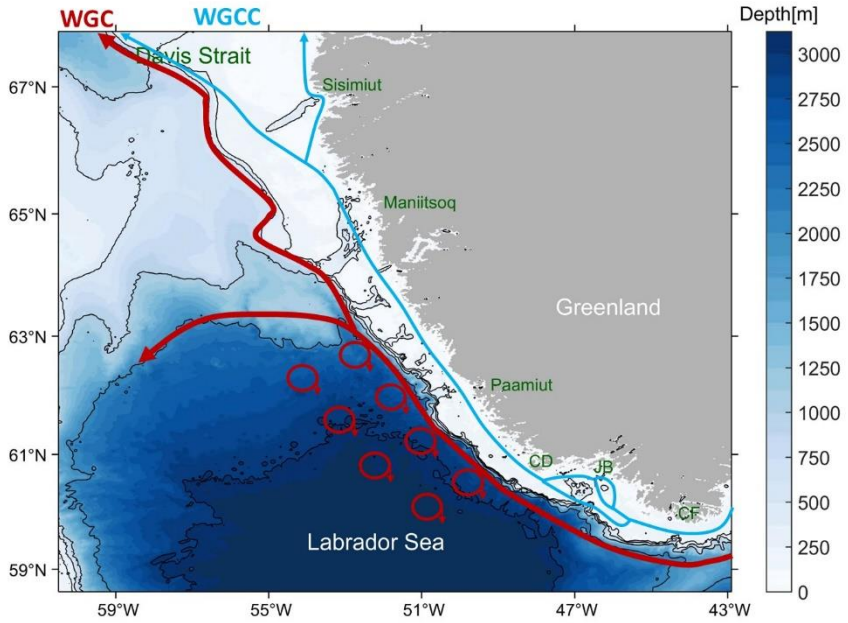

Figure 1. Schematic showing the geographical features and mean circulation pathways off the west Greenland coast. The blue and red arrows correspond to the WGCC and WGC respectively, and the red circles denote eddies shed by the WGC. CF, JB, CD, denotes Cape Farewell, Juliannehaab Bight, Cape Desolation respectively. The black contour lines indicate the 250, 500, 1,000, 2,000, and 3,000 m isobaths and the contour interval is non-linear.

2 Model and Method Description

2.1 Model

The model used in this study is based on the NEMO numerical framework, version 3.6 (Madec, 2008). It has an inner nest of 1/60° resolution in the Labrador Sea, with a couple of outer nests covering the Arctic and the North Hemisphere Atlantic (ANHA; Hu et al., 2018) and the sub-polar gyre (Pennelly and Myers, 2020). In our study area, the horizontal resolution is around 800~1100 m. Thus only within this nest can the model resolves the first baroclinic Rossby radius on the shelf (Gou et al., 2021). The atmospheric forcing has been changed to Drakkar Forcing Set 5.2 (DFS5.2; Dussin et al., 2016), instead of the Canadian Meterological Centre's Global Deterministic Prediction System ReForecast product (CGRF; Smith et al., 2014) used in Gou et al. (2021), to better represent convection in the Labrador Sea (Pennelly and Myers, 2021). Ten-years of output from 2008 to 2018 saved as daily averages are used in this study. The vertical mesh consists of 75 layers with ~1 m resolution at the surface that decreases with depth, and the top 250 m is made up by 34 layers. The implementation of the simulation, the initial and boundary conditions, and other forcings, are explained in Gou et al. (2021). For further details of the model setup, please refer to Pennelly and Myers (2020).

2.2 Transport calculation

We look into the current transports at eight observational sections (Figure 2): OSNAP West (Lozier et al., 2017), the Greenland Institute of Natural Resources (GINR) standard

sections – Cape Farewell, Cape Desolation, Fylla Bank, Maniitsoq, Sisimiut (Mortensen, 2018), and the regularly sampled WOCE AR7W line (Hall et al., 2013). We extend the sections onshore to cover the coastal current, and extend the northern three sections offshore to cover the whole WGC (Figure 2).

The transports are defined to be positive when they are directed to the north and northwest along the main axis of the west Greenland shelf. The WGCC transports are based on integrating the model velocity fields perpendicular to each section where the bathymetry is shallower than 250m (see Figure 1) and WGC transports are based on integrating farther offshore where the speed is larger than 0.1 m/s and the salinity is smaller than 34.8. Focusing on the freshwater component of the WGC instead of its Irminger water component, we thus apply the 34.8 isohaline to denote the edge of the WGC as Myers et al. (2009) did. Since eddies are generated and shed by the WGC between Cape Desolation and Fylla Bank, for these sections, the WGC transport integrals are defined to only include those grid points where the velocity direction is northward along the coast. Since the speed of the WGC begins to slow at Maniitsoq and Sisimiut, and the offshore parts of the sections may capture the southward flow near the western boundary, for these sections, the definition for the WGC transport is changed to integrating offshore from the WGCC to where the salinity is smaller than 34.8 and the velocity direction is northward along the coast. We calculate the freshwater transports and heat transports based on multiple reference values, due to the variety of them used in different studies (Gou et al., 2021). We only present the results referenced to 34.8 salinity and -1.8°C temperature in this manuscript, with the results referenced to other values in the supplementary material (Figures S1-S4).

2.3 Method for analyzing the forcing mechanisms

We apply the method from Whitney and Garvine (2005) that computes the wind-forced velocity components (u_w) and buoyancy-forced velocity components (u_b) of the currents. u_w is induced by the wind-forced sea surface height gradient and u_b is induced by the horizontal density gradient. The wind strength index (W_s), the ratio between the u_w and u_b, denotes the relative importance between wind and buoyancy forcing. When $|W_s|$ is >1, the current is predominantly wind-driven. And when $|W_s|$ is <1, the current is predominantly buoyancy-driven.

This method has been applied to the EGCC, using observations (Sutherland & Pickart, 2009) and modelling (Bacon et al., 2014). And it has been applied in the observational study of the WGCC by Lin et al. (2018). Here, we follow the application of this method by Bacon et al. (2014) as our study also uses a numerical model.

The wind-forced velocity component u_w is defined as

$$u_w = \sqrt{\frac{\rho_{air}}{\rho}\frac{C_{10}}{C_D}} \cdot U$$

where ρ_{air} is air density set as a constant of 1.293 kg/m^3, ρ is water density set as a constant of 10^3 kg/m^3, $C_{10} = 10^{-3}(\frac{2.7}{|U|} + 0.142 + \frac{|U|}{13.09})$ is the surface drag coefficient, C_D is the bottom drag coefficient set as a constant of 10^{-3}, and U is the along-shelf 10-m wind speed (the component normal to the section) from DFS5.2 over the period of 2008-2017. U is averaged over the

coordinate points comprising each section that covers the width of each current, and |U| is its absolute value.

The buoyancy-forced velocity component u_b is defined as

$$u_b = \frac{R_1}{W}(2g'Qf)^{1/4}$$

where R_1 is the first baroclinic Rossby radius, W is the width of the current, g' is the reduced gravity, Q is the volume transport of the current, and f is the Coriolis parameter set as a constant of 1.3×10^{-4} s^{-1}. Specifically, $R_1=NH/f\pi$ is calculated at the location of the maximum of the top-250 m averaged speed, where H denotes the full water depth for the WGCC or the depth where the salinity is below 34.8 for the WGC. $N^2 = -(\frac{g}{\rho})\frac{\partial \rho}{\partial z}$ is the buoyancy frequency and $\frac{\partial \rho}{\partial z}$ is estimated as the density difference between the surface layer and the layer with a depth of H, divided by H (i.e. delta z). W is the distance between the points where the speed falls to 70% of the maximum. The densities at those points are used to estimate $g'=g(\rho_2-\rho_1)/\rho_1$, where g is set to be 9.8 m s^{-2} and ρ_2 is on the offshore side. These densities are computed at 75 m depth, except at Fylla Bank and Sisimiut, where the surface layer is used as the continental shelf of these two sections are very shallow. Note that at the Fylla Bank and Sisimiut sections, as the currents are not coherent, and do not have a clear core that their speeds decline away from. Thus, to define W, the currents were divided into several branches when calculating W. So for these two sections, W and corresponding g' are the sum of the W and g' of each branch. To avoid the southward flow in the west Labrador Sea at Sisimiut, only the offshore 180 km of the section are included in the calculation for that section.

3 Speeds

3.1 Annual mean strucutre

We first look at the top-50 m model annual mean speed field off the west Greenland coast, averaged over 2008-2018 (Figure 2). The WGCC remains coherent with a strong year-round on-shelf jet from the Cape Desolation section almost to the Paamiut section. Significant flow remains on the shelf north to the Sisimiut section and Davis Strait. Bands of narrow flow with annual mean velocities exceeding 0.1 m s^{-1} can be seen in the deeper water inshore of the various banks interspaced with regions of broader and weaker flow, consistent with the observed shelf flow around the Fylla Bank section (Myers et al., 2009). In the annual mean, the flow separates on the shelf between the Maniitsoq and Sisimiut sections, with most of the flow moving towards the shelf-break as the Sisimiut section is approached. The mean velocities inshore of the Maniitsoq section are close to 0.1 m s^{-1}, and those at the Sisimiut section are generally lower than 0.05 m s^{-1}, same as indicated by Myers et al. (2009). For further comparison, a direct meansurement of the northward surface velocity on the west Greenland shelf across the Davis Strait is 0.06 m s^{-1} while an estimate using hydrographic data is 0.02 m s^{-1} (Azetsu-Scott et al, 2011). And the shelf velocity was observed to reach 0.1 m s^{-1} during 1987-1990 (Cuny et al., 2005).

The WGC continues north as a strong current with annual mean core velocities exceeding 0.5 m s^{-1} until the Paamiut section, where there is a broad region with velocities exceeding 0.2 m s^{-1}. Northward to the Fylla Bank section, the continental slope gets flatter as the 2000m and 3000 m isobaths veer westward sharply. Correspondingly, the WGC splits into two branches at

the Fylla Bank section, with the major one along the 2000 m isobath, eventually joining the Labrador Current with velocities reaching 0.2 m s^{-1}, and a narrower, weaker branch heading northward to Davis Strait and into Baffin Bay. Considering the fact that currents follow the f/H contours (f denotes Coriolis parameter and H denotes the bottom depth), the mean path of the northward branch largely follows the curving 500 m isobath close to the west Greenland shelf break, thus interacting with the observed southward flows that veer eastward from the western strait (Cuny et al., 2005; Curry et al., 2011; Curry et al., 2014). These phenomenon in the model also correspond to what was found in the observational study by Myers et al. (2009). And the paths of the WGCC and WGC from the Cape Farewell section to Davis Strait were similarly illustrated by Curry et al. (2014). The annual speeds of this northward branch could be as low as below 0.05 m s^{-1}, and as high as above 0.15 m s^{-1}. Stein (2004) had estimated that the speed of the WGC flowing through the Davis Strait is in the range of 0.1-0.36 m s^{-1}. The modelling study by Lique et al. (2009) suggested that the WGC speed across the Davis Strait could reach 0.1 m s^{-1}. And a recent observational study by Majumder et al. (2021) has shown that the speed of the WGC flowing from 61°N to 64-65°N is approximately 0.17 m s^{-1}.

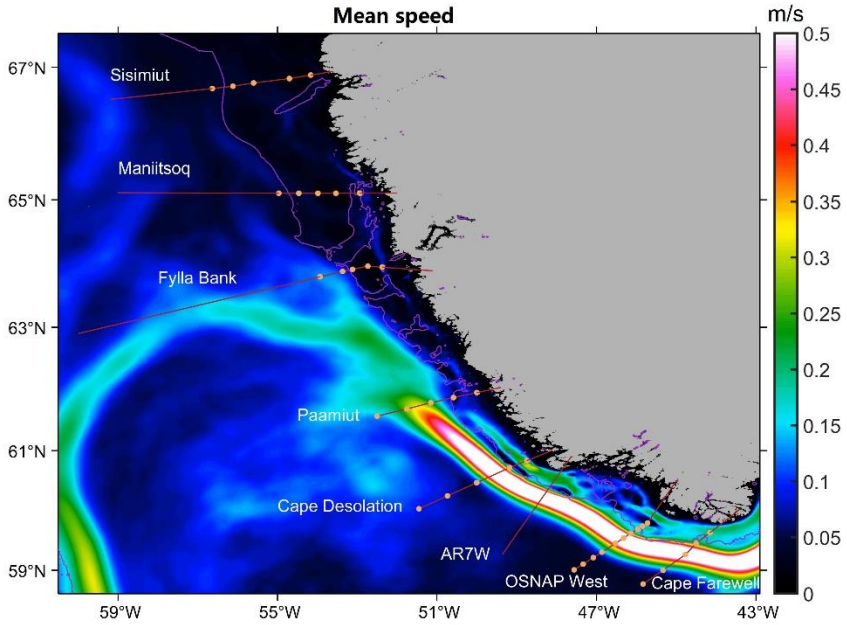

Figure 2. Mean model top-50m speed field off the west Greenland coast for 2008-2018. Sections are shown by red lines, with yellow dots representing the actual stations, and the purple lines denote the 250m isobath.

3.2 Inter-annual variability

It is noted that north of Fylla Bank in 2010, the WGC and WGCC have speeds of ~0.15 m s^{-1} and ~0.1 m s^{-1} respectively (Figure S5), which are the highest in the ten-year period. This anomaly is also reflected in Figure 3 revealing the annual anomaly, showing that the speed increases of the northern WGCC and WGC reached ~0.05 m s^{-1} and ~0.1 m s^{-1} respectively, that year. This is related to anomalous winds off the west Greenland coast in 2010, which led to anomalously large northward Ekman transport, increasing the transport of the WGC north through Davis Strait (Myers et al., 2021).

It is seen from Figure 3 that, south of Fylla Bank section, the speed anomaly of the WGCC becomes negative in the later years, while the negative speed anomaly of the WGC turns to positive correspondingly. Therefore, the inter-annual trend of the WGCC speed is opposite to that of the WGC over 2008-2018. The WGCC weakens by more than 0.1 m s^{-1} as the WGC strengthens with a speed increase that approaches 0.2 m s^{-1}. This relation is especially noticeable south of Paamiut section, where the WGC is stable and does not shed eddies. North of Fylla Bank section, for both currents, the general speed anomaly does not follow the same pattern, both in terms of the magnitude and inter-annual variations. For example in 2010, there is a large positive speed anomaly for the northern WGC but large negative speed anomaly to the south. Furthermore, the difference between the north and south implies that the forcing mechanisms of the currents north of Fylla Bank section may be different from those to the south.

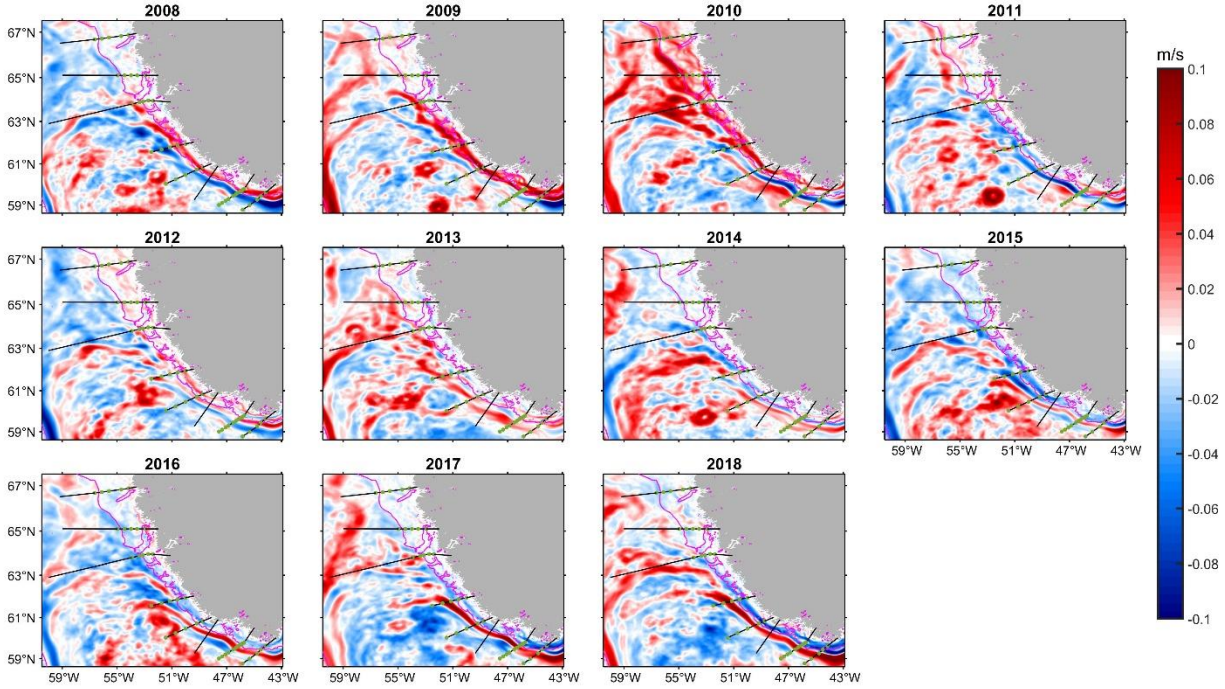

Figure 3. Annual anomalies of the top-50m speed field for the given years referenced to the 2008-2018 mean. Sections are shown by black lines, with green dots representing the actual stations, and the magenta lines denote the 250m isobath.

4 Transports

4.1 Annual mean transports

The time-mean transports of the WGCC are presented in Figure 4. In comparison with the same model driven by different atmospheric forcing (see Table 1 in Gou et al. (2021)), differences are larger to the south, with the volume transport at Cape Farewell section being 0.14 Sv smaller and 0.07 Sv smaller at the OSNAP West section. For the AR7W and Cape Desolation sections, the differences are negligible. The model sensitivity to the atmospheric forcing is strongest near Cape Farewell and maybe related to the inflows into the inner nest. Our time-mean volume transports of the WGC for 2008-2018 (Figure 4a) are in the ranges of the

means for 1984-2005 shown by Myers et al. (2009), except for larger values at Fylla Bank (3.5 Sv versus 1.1±0.9 Sv) and Maniitsoq (1.2 Sv versus 0.1±0.2 Sv). This could be due to the fact that we include the unstable part of the WGC that sheds eddies at Fylla Bank, and a part of the WGC at Maniitsoq is located in the extended part of the section in this analysis.

Our time-mean freshwater transports are generally larger than Myers et al. (2009)'s results (e. g., 81.9 mSv versus 45.8±11.8 mSv at Cape Farewell, 84.3 mSv versus 47.7±12.3 mSv at Paamiut, and 12.2 mSv versus 0.03±5.4 mSv at Sisimiut) with the differences smallest at the Cape Desolation section (78.0 mSv vs 54.4±22.4 mSv). A speculation for the larger transports seen in this study is that the subarctic has undergone notable freshening, consistent with Arctic and Greenland warming and melting (Dukhovskoy et al., 2019). Additionally it may be that the Myers et al. (2009) values were biased low because of a poor representation of the low salinity flows on the shelf. In terms of mean heat transports referenced to 0°C (Figure S4), other than the differently defined Fylla Bank and Maniitsoq sections, our results are generally in the ranges of those presented by Myers et al. (2009). The exception is the Paamiut section where our heat transport of greater than 60 TW is much larger than the previous estimate of 25±13 TW.

For both the WGCC and WGC at the Sisimiut section, the combined model mean volume transport (0.45 Sv) and freshwater transport (16.4 mSv) (Figure 4) are very close to the Davis Strait transport estimates from previous observational studies, despite different definitions for the transport integrals. For instance, Curry et al. (2011) showed that the mean volume and freshwater transport (referenced to a salinity of 34.8) for the west Greenland shelf for 2004-2005 are 0.4 Sv and 15 mSv respectively. Another study by Curry et al. (2014) found that the mean volume and freshwater transport (referenced to a salinity of 34.8) of the West Greenland Shelf Water (recognized as the WGC; potential temperature<7°C; salinity<34.1) for 2004-2010 was 0.4 Sv and 17 mSv respectively. Their heat transport (referenced to 0°C) was computed to be 3 TW, which is smaller than our combined heat transport of 4.8 TW (Figures S3 and S4).

4.2 Transport losses and exchanges

Despite the splitting and re-combination of the WGCC on the shelf between OSNAP West and AR7W (Gou et al., 2021), there is no loss in the volume or freshwater transport between those two sections. The same is true for the WGC between these sections. Continuing north to the Cape Desolation section, there is little change in the total northward transport (Figure 4). However, offshore exchanges leads to the WGCC losing 0.07 Sv and 4.0 mSv of it volume and freshwater transports, respectively to the WGC. Given that Pacini and Pickart(2021) observe significant meandering of the WGC at OSNAP West, it is likely that those meanders are then damped, given the transport coherence to Cape Desolation.

The observational study by Myers et al. (2009) showed the most significant exchange from the WGC to the Labrador Sea interior occurs between Cape Desolation and Fylla Bank. Majumder et al. (2021) has also pointed out that the offshore transport from the coast to the interior Labrador Sea mainly occurs at 61°N-62°N. Irminger Rings are also formed and exchange waters offshore in this region (Katsman et al., 2004). Although we see such offshore exchange, the ability to see more details of the currents with the high-resolution models shows us that the situation in this region is more complex. Offshore exchange from the shelf, likely due to Ekman transport, reduces the WGCC volume transport by over 50% between the Cape

Desolation and Paamiut sections, with a further reduction to 0.07 Sv by the Fylla Bank section. Similar reductions are see (Figure 4). Similar loses are seen for the WGCC's freshwater and heat transport.

Given the offshore losses by the WGCC are into the WGC, this additional waters masks the offshore loses from the WGC (Figure 4). Although the volume transport of the WGC drops only 0.3 Sv between the Cape Desolation and Paamiut sections, the total offshore exchange of water between those same two sections is 0.5 Sv. Similarly the boundary current system loses a total of 1.4 sv between the Cape Desolation and Fylla Bank sections. Interestingly, the WGC's freshwater transport increases from the Cape Desolation to Paamiut sections, with only a small drop through to the Fylla Bank section (Figure 4). However, given the significant loses from the WGCC, in actual fact we seen a long term mean offshore freshwater transport of 13 mSv in this region. The offshore exchange of heat is more consistent with the changes in the volume transport, with 36.7 TW of heat fluxed into the interior of the Labrador Sea south of the Fylla Bank section.

Myers et al. (2009) found warm season transports across the Fylla Bank section of 1.0 Sv and 23.0 mSv. Yet, we find a long term mean transport of the WGC across the Fylla Bank section of 3.5 Sv and 83.1 mSv (Figure 4). The reason for the difference is the extension of our section in this analysis to catch the significant transport following the isobaths around the northern rim of the Labrador Sea. Similarily, we find a WGC transport north across the Maniitsoq section of 1.2 Sv while Myers et al. (2009) found close to zero. Again, our use of an extended section captures transport continuing farther northward along the eastern margin of the Labrador Sea before turning westward. The remaining 0.4 Sv we see at the Sisimiut section is therefore the model's long term mean transport for the WGC into Baffin Bay, supplemented by 0.05 Sv by the WGCC on the shelf.

Similarly, for freshwater transport, the precipitous decreases seen in Myers et al (2009) for the Fylla Bank and Maniitsoq sections compared to the Cape Desolation section are related to the short length of the northern observational sections used, rather than a near complete exchange of all the freshwater from the WGC into the interior of the Labrador Sea. Although there is little net northward freshwater transport into Baffin Bay on the shelf, 12.2 mSv enter that basin via the WGC. And the majority of the freshwater (over 80 mSv) carried north in the WGC, crosses the Fylla Bank (and the Maniitsoq section for a significant fraction) before turning west and circulating around the northern Labrador Sea. And although we don't look at exchange into the Labrador Sea interior from its northern end, other studies (Schulze-Chretien and Frajka-Willians, 2018; Pennelly and Myers, 2019) find little such exchange in this northern region.

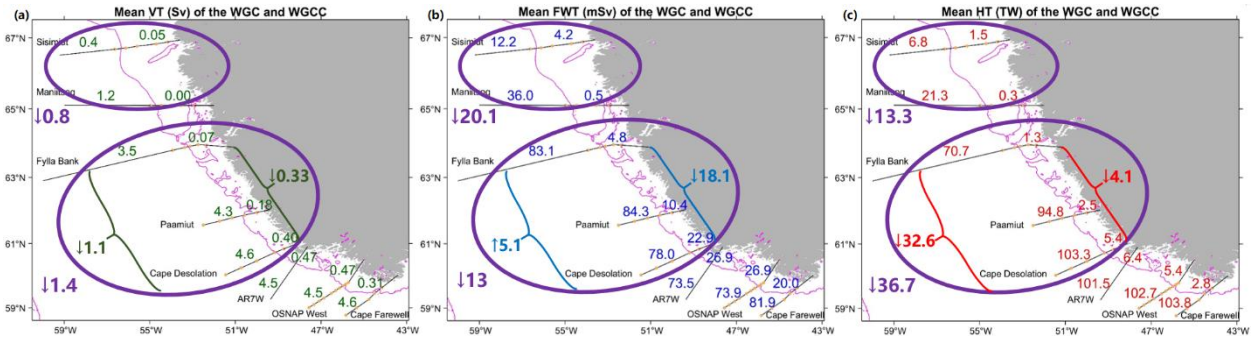

Figure 4. Schematic showing the annual means (2008-2018) of the volume transport (a), freshwater transport (b), heat transport (c) for each section. The WGCC transports are denoted by the numbers inshore of the 250 m isobath (magenta line), and the WGC transports are denoted by the numbers offshore of the 250 m isobath. The transport losses of the WGCC and WGC from Cape Desolation to Fylla Bank are labelled by offshore and onshore braces, respectively. The total transport losses between sections are labelled by the pirple circles and numbers.

4.3 Inter-annual variability

Inter-annual events previously discussed are also reflected in the timeseries of the WGCC (Figure 5) and WGC (Figure 6) transports. The WGCC transports at Sisimiut and WGC transports at Maniitsoq are anomalously high in 2010, being ~0.3 Sv and ~1 Sv respectively larger than the mean. Another peak of the WGCC freshwater transport at the northern three sections is seen in 2012, while the WGC freshwater transports at these sections are minimal values. 2012 is a year with record Greenland melt (Nghiem et al., 2012; Tedesco et al., 2013), and the downwelling favorable winds during that year likely constrained the meltwater near the coast and transported it northward to the Baffin Bay (Luo et al., 2016).

To the south of Fylla Bank, the trend of the WGC volume transport is opposite compared to the WGCC, though the variations from year to year may not correspond perfectly. There is unexpected southward WGCC transport of 0.05 Sv at Sisimiut and Maniitsoq in 2015 and 2016. This is consistent with the assumption made by Rysgaard et al. (2020) based on an observational water mass analysis, that southward coastal current transports exists in 2015 and 2016 south of Davis Strait.

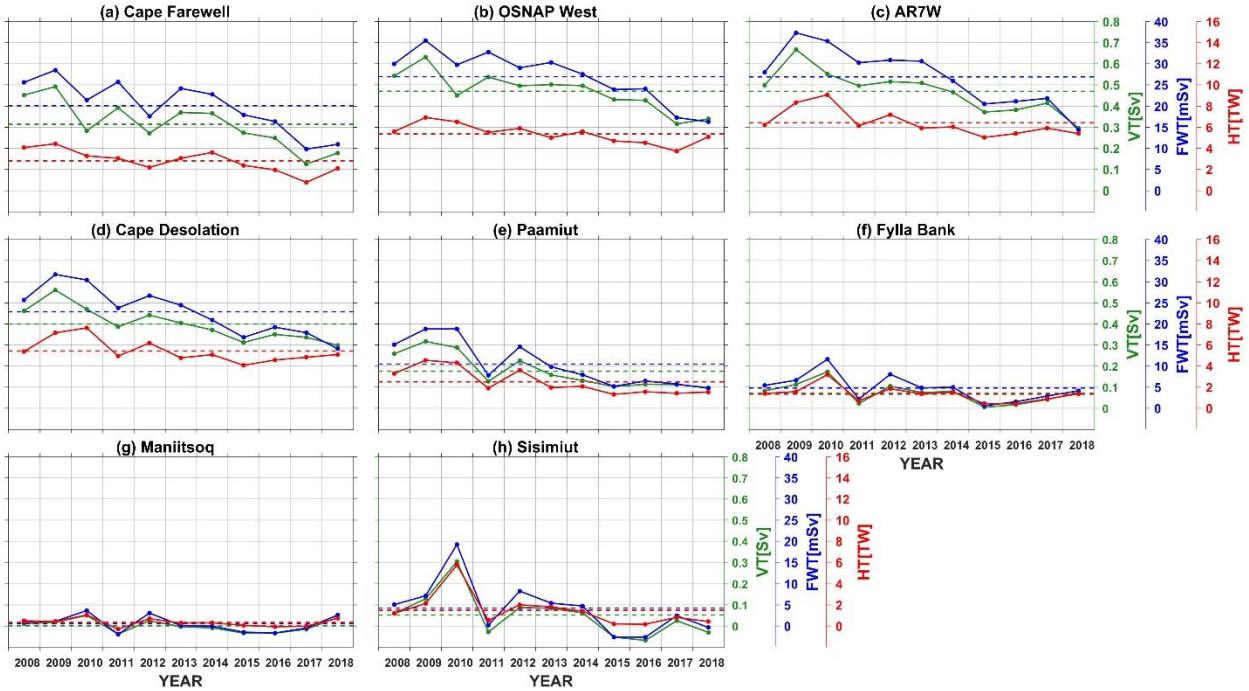

Figure 5. Annual WGCC transports with dashed lines denoting long-term means over 2008-2018. Green, blue, red lines and y-axes correspond to volume transports (VT), freshwater transports (FWT), heat transports (HT) respectively. Each of the sections are identified in Figure 1b.

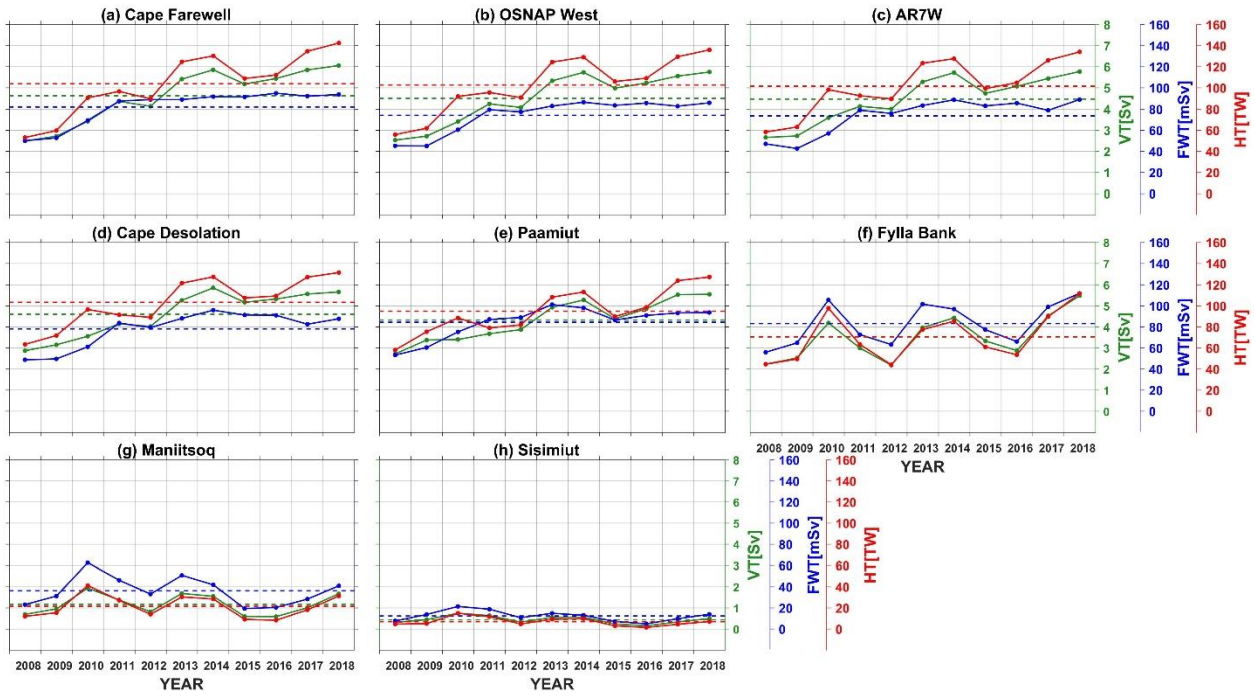

Figure 6. Same as Figure 2 but for the WGC.

5 The Forcing Mechanisms

We now explore the forcing mechanisms of the currents and try explaining their inter-annual variability. The monthly u_w and u_b of the WGCC at the Cape Desolation section are shown in Figure 7a. As u_w is mostly negative throughout the ten-year period except in summer, upwelling favorable winds should prevail in this region that counter the buoyancy-driven flow (Whitney & Garvine, 2005). While during 2010 when u_w is mostly positive, downwelling favorable winds prevail that augment the flow (Whitney & Garvine, 2005). This wind pattern and its anomaly in 2010 corresponds to those indicated by Myers et al. (2021).

The decreasing trends of both the u_b and u_w could largely explain the decreasing trends of the WGCC transports. As $|W_s|$ is mostly <1 throughout the whole period with a mean of ~0.5 (Figure 7b), the WGCC is predominantly buoyancy driven. And when the wind is downwelling favorable (W_s >0), $|W_s|$ is mostly <0.5. While when the wind is upwelling favorable (W_s <0), the frequency of events with $|W_s|$>0.5 or even $|W_s|$>1 is significantly more likely. Therefore, the possibility of anomalously strong upwelling favorable winds is larger than that for the downwelling favorable winds, thus having a larger impact on the WGCC overall.

Using shipboard data in summer 2014, Lin et al. (2018) evaluated the $|W_s|$ for the coastal current rounding Cape Farewell in the vicinity of the south Greenland, finding a mean of 0.18 and a range of 0.05-0.41. Sutherland & Pickart (2009) showed that the $|W_s|$ for the EGCC at an observational section just east of Cape Farewell, in the summers from 1997 to 2004, was in the range of 0.02-0.5, although except for being 0.5 at Cape Farewell in summer 2003, the $|W_s|$ was below 0.25. They showed that the $|W_s|$ for the EGCC at sections north of Cape Farewell in summer 2004 in the range of 0.05-0.25. Our $|W_s|$ of the WGCC in summer is generally lower than that in other seasons (Figure 7b), so it is generally lower than the mean $|W_s|$ and corresponds

well with these observational results, though there may be differences in wind and buoyancy forcings between the west and east Greenland shelf. Note that Bacon et al. (2014)'s modelling results showed that the $|W_s|$ of the EGCC as close to 1 so that wind and buoyancy forcing were similarly important to the EGCC.

In terms of the velocity components of the WGC at Cape Desolation (Figure 7c), its u_w is basically the same as that of the WGCC (Figure 7a), as the wind does not change much over the small spatial scale between shelf and shelfbreak current. Meanwhile u_b steadily increases over 2008-2018. The W_s of the WGC (Figure 4d) has similar features as that of the WGCC (Figure 7b), as indicated above, with a $|W_s|$ of ~0.4. So the WGC at Cape Desolation is also predominantly buoyancy driven. And the increasing trend of the u_b could largely explain the trend of the WGC transports discussed above (Figure 3).

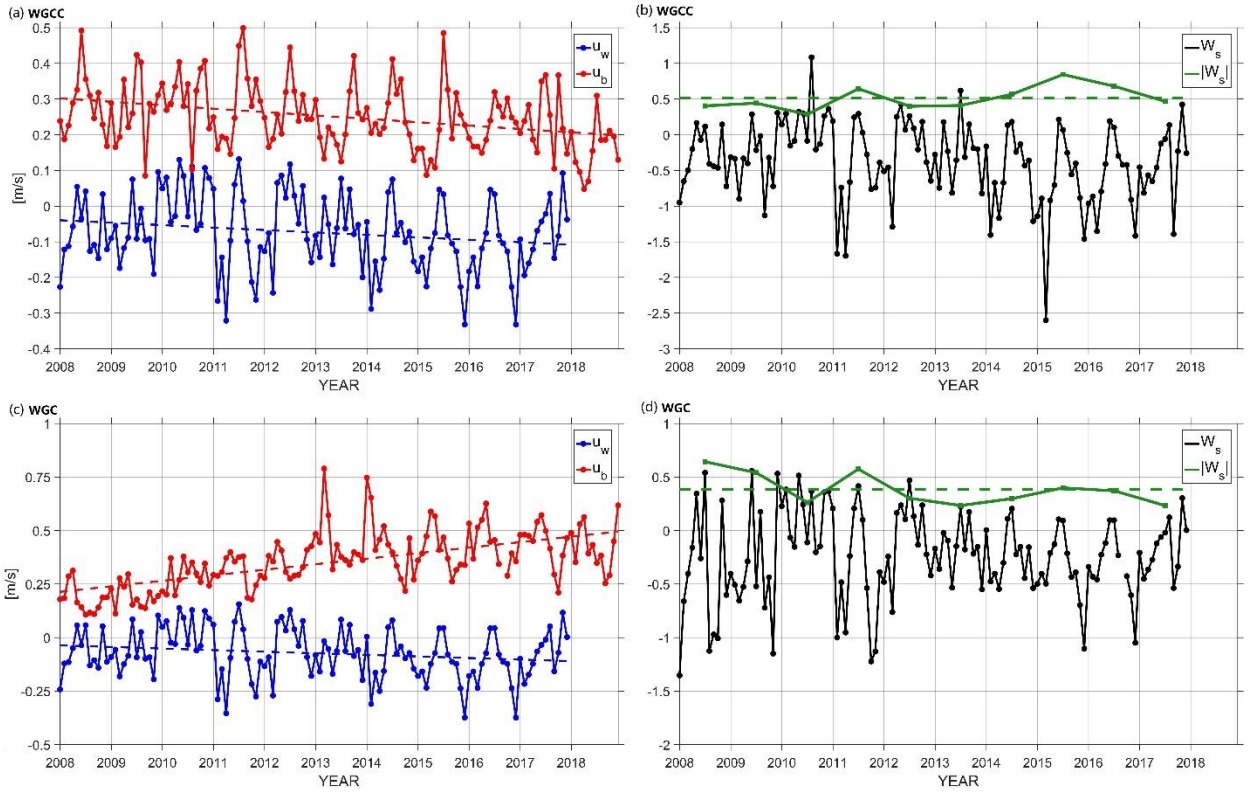

Figure 7. The monthly u_w (blue solid line) and u_b (red solid line) of the WGCC (a) and WGC (c) at Cape Desolation, with dashed lines denoting their linearly regressions. And the monthly W_s (black line) and its annual absolute value (green line) of the WGCC (b) and WGC (d) at Cape Desolation, with the dashed green lines denoting the time-mean absolute values.

To the north of Cape Desolation, the forcing mechanisms of the currents change. The u_w term is similar among the sections, consistent with large atmospheric scales. But the buoyancy terms evolve, changing the relative importance between wind and buoyancy forcing. At Fylla Bank, as the frequency of $|W_s|>1$ and that of $|W_s|<1$ are both high (Figure S6b and S6d), wind forcing and buoyancy forcing both become important to the WGCC and WGC, though the frequency of $|W_s|<1$ for the WGCC is much larger before 2009. Similarly, at Sisimiut, wind forcing and buoyancy forcing are both important to the WGCC (Figure S7b), while the wind

forcing is dominant in forcing the WGC as $|W_s|$ is mostly >1 (Figure S7d). In all cases indicated in this paragraph, the time-mean $|W_s|$ is much larger than 1, since extremely large $|W_s|$ exists sometimes, especially when $W_s<0$.

6 Discussion and Conclusions

Using ten-years of output from a high-resolution (1/60°) numerical model, we presented the inter-annual variability of the WGC and WGCC in terms of their speeds, transports and forcing mechanisms.The WGCC and WGC are found to extend to Davis Strait during most years, especially during 2010 when the current speeds and transports are the highest in the study period. This could be due to the anomalous wind pattern in 2010 (Myers et al., 2021). The freshwater transports of the WGCC at the northern three sections showed maximums in 2012, which could be the result of the record Greenland melt and downwelling favorable winds in that year (Nghiem et al., 2012; Tedesco et al., 2013; Luo et al., 2016). While in 2015 and 2016, the transports of the WGCC at Sisimiut and Maniitsoq are southward, consistent with the assumption made by Rysggard et al. (2020). And at southwest Greenland, the inter-annual trends of the speeds and transports of the WGCC are opposite to those of the WGC, with the WGCC declining and the WGC strengthening, over 2008-2018.

At Cape Desolation where large Greenland runoff exists, the WGCC and WGC are both predominantly buoyancy forced, and their buoyancy forced velocity components largely explains their transport variability. At Fylla Bank and Sisimiut, the wind forcing is more dominant, and the WGCC and WGC are forced by both wind and buoyancy except that the WGC at Sisimiut is predominantly wind forced. Generally, upwelling favorable winds provide a stronger forcing than downwelling favorable winds.

Since both the WGC and WGCC are predominantly buoyancy-forced at Cape Desolation, their opposite trends in inter-annual variability implies the opposite impacts from Greenland and Arctic melt on the currents, which could change horizontal density gradients across the currents and thus their u_b. There are areas like Juliannehaab Bight in the southwest Greenland (Figure 1a) that have significant Greenland melt discharge. And the WGC and the WGCC are the extentions of the East Greenland Current and EGCC, which originate from Fram Strait where large Arctic outflows pass through (Bacon et al., 2014; Sutherland & Pickart, 2009). In terms of the Greenland melt, the model experiment by Dukhovskoy et al., (2019) has shown a considerable lateral advection of the Greenland melt from the southwest Greenland shelf to the interior Labrador Sea. It was also suggested that the Greenland melt would be intensively vertically mixed as crossing the shelf.

The transport decrease along the coast suggests substantial exchanges from the current system into the interior and northern Labrador Sea region. And the main exchange into the interior occurs between Cape Desolation and Fylla Bank, with the WGCC being the main freshwater source. The density anomalies in the Labrador Sea are mainly thought to be originated from the eastern subpolar gyre (Li et al., 2021), however, the exchange into the interior Labrador Sea also could generate density anomalies. The freshwater and heat inflows of 13 mSv and 36.7 TW from the current system play nonnegligible roles in setting the preconditioning and restratification of the deep convection. Yet, as we show, the majority of the freshwater (~87%) and heat (~66%) in the combined WGC/WGCC current system are transported into the northern part of the basin, past the Fylla Bank section (Fig. 4), where they likely circulate around the basin, before flowing south with the Labrador Current. This is also

consistent with tracer and virtual Lagrangian float studies that show most of the freshwater coming from the Greenland icesheet reaches the northern Labrador Sea and/or the Labrador current rather than the interior convective patch (Gillard et al., 2016, Luo et al., 2016). This may be why higher resolution model studies generally do not find a significant impact of Greenland freshwater on Labrador Sea water formation as of yet (e.g. Böning et al., 2016). Poor representation of the WGCC and shelf processes may lead to low salinity water being farther offshore in coarse resolution models and thus easier to exchange into the interior. For example, based on a 1/12th degree simulation functionally equivalent to the intermediate nest used here, Pennelly and Myers (2019) found a long-term (2006–2016) annual mean exchange of 21 ± 11 mSv of freshwater (also relative to 34.8) across the 2,000-m isobath to the interior of the Labrador Sea. Which is almost double our estimate of 13 mSv over 2008-2018, which is unlikely to be due to the small difference in averaging period.

Limited exchange of freshwater into the Labrador Sea interior is also consistent with strong deep convection occurring in the Labrador Sea in recent winters (Yashayaev and Loder, 2016). Thus, even if a warming climate leads to continued enhancement in Greenland and Arctic melt and an increase in transport in the WGC system, it is open question if a significant component of that increase will reach the convective portion of the interior of the Labrador Sea. It is possible such additional low salinity water may accumulate in Baffin Bay, although Dukhovskoy et al. (2021) suggests that the sub-polar interior will be more sensitive to enhanced freshwater from the southwest Greenland shelf. If much of the recent increases in Greenland melt (Bamber et al., 2018) was not lost to the interior of the Labrador Sea, but followed the boundary current system around the Labrador Sea, there is potential that this water contributed to the record sub-polar gyre freshening event between 2012 and 2016 that Holliday et al. (2020) reported on.

Acknowledgments

The authors declare no competing financial interests. This work was funded by Natural Sciences and Engineering Research Council of Canada (NSERC) grants awarded to PGM. These include Discovery Grants (rgpin 227438-09 and 2020-04344) and a Climate Change and Atmospheric Research Grant (433898). GLORYS reanalysis received support from Mercator Ocean, Groupe Mission Mercator Coriolis and the European Community's Seventh Framework Programme FP7/2007-2013 under Grant Agreement number 218812 (MyOcean). The authors would like to thank the NEMO development team as well as the DRAKKAR group for providing the model code and continuous guidance.

The Fortran code used to carry out the LAB60 simulation can be accessed from the NEMO version 3.6 repository (https://forge.ipsl.jussieu.fr/nemo/browser/NEMO/releases/release-3.6 , last access: 14 October 2020). A few Fortran files were modified to handle our passive tracers. The complete Fortran files as well as the CPP keys, namelists, and associated files can be found on Zenodo (https://doi.org/10.5281/zenodo.3762748, Pennelly, 2020). Due to the large storage demands for a 1/60 degree resolution simulation with daily output that spans 14 years, the initial and boundary conditions, atmospheric forcing, and numerical output remains on the high performance computing platform Compute Canada. We express our thanks to Compute Canada (http://www.computecanada.ca) for the computational resources to carry out our numerical simulations as well as archival of the experiments.

References

Azetsu-Scott, K., Petrie, B., Yeats, P. & Lee, C. (2012). Composition and fluxes of freshwater through Davis Strait using multiple chemical tracers, *Journal of Geophysical Research: Oceans*, *117*, C12011. doi:10.1029/2012JC008172.

Bacon, S., Marshall, A., Holliday, N. P., Aksenov, Y., & Dye, S. R. (2014). Seasonal variability of the East Greenland Coastal Current. *Journal of Geophysical Research: Oceans*, *119*(6), 3967–3987. doi:10.1002/2013JC009279

Bamber, J. L., Tedstone, A. J., King, M. D., Howat, I. M., Enderlin, E. M., van den Broeke, M. R., & Noel, B. (2018). Land ice freshwater budget of the Arctic and North Atlantic Oceans: 1. Data, methods, and results. *Journal of Geophysical Research: Oceans*, *123*, 1827–1837. doi:10.1002/2017JC013605

Böning, C. W., Behrens, E., Biastoch, A., Getzlaff, K., & Bamber, J. L. (2016). Emerging impact of Greenland meltwater on deepwater formation in the North Atlantic Ocean. *Nature Geoscience*, 9(7), 523-527.

Bracco, A., Pedlosky, J., & Pickart, R. S. (2008). Eddy formation near the west coast of Greenland. *Journal of Physical Oceanography*, *38*(9), 1992–2002. doi:10.1175/2008JPO3669.1

Castelao, R. M., Luo, H., Oliver, H., Rennermalm, A. K., Tedesco, M., & Bracco, A., et al (2019). Controls on the transport of meltwater from the southern Greenland ice sheet in the Labrador Sea. *Journal of Geophysical Research: Oceans*, *124*, 3551–3560. doi:10.1029/2019JC015159

Castro de la Guardia, L., Hu, X., & Myers, P. G. (2015). Potential positive feedback between Greenland Ice Sheet melt and Baffin Bay heat content on the west Greenland shelf. *Geophysical Research Letters*, *42*, 4922–4930. doi:10.1002/2015GL064626.

Cuny, J., Rhines, P. B., & Kwok, R (2005). Davis Strait volume, freshwater and heat fluxes. *Deep Sea Research Part I: Oceanographic Research Papers*, *52*(3), 519-542. doi:10.1016/j.dsr.2004.10.006.

Curry, B., Lee, C. M., & Petrie, B. (2011). Volume, Freshwater, and Heat Fluxes through Davis Strait, 2004–05, *Journal of Physical Oceanography*, *41*(3), 429-436. doi:10.1175/2010JPO4536.1

Curry, B., Lee, C. M., Petrie, B., Moritz, R. E., & Kwok, R. (2014). Multiyear Volume, Liquid Freshwater, and Sea Ice Transports through Davis Strait, 2004–10, *Journal of Physical Oceanography*, *44*(4), 1244-1266. doi:10.1175/JPO-D-13-0177.1

de Jong, M. F., Bower, A. S., & Furey, H. H. (2014). Two years of observations of warm-core anticyclones in the Labrador Sea and their seasonal cycle in heat and salt stratification. *Journal of Physical Oceanography*, *44*(2), 427–444. doi: 10.1175/JPO-D-13-070.1

Dukhovskoy, D. S., Myers, P. G., Platov, G., Timmermans, M. L., Curry, B., Proshutinsky, A., et al. (2016). Greenland freshwater pathways in the sub-Arctic Seas from model experiments with passive tracers. *Journal of Geophysical Research: Oceans*, *121*(1), 877–907. doi:10.1002/2015jc011290

Dukhovskoy, D. S., Yashayaev, I., Chassignet, E. P., Myers, P. G., Platov, G., & Proshutinsky, A. (2021). Time Scales of the Greenland Freshwater Anomaly in the Subpolar North Atlantic. *Journal of Climate*, 34(22), 8971-8987. doi:10.1175/JCLI-D-20-0610.1.

Dukhovskoy, D. S., Yashayaev, I., Proshutinsky, A., Bamber, J. L., Bashmachnikov, I. L., Chassignet, E. P., et al. (2019). Role of Greenland freshwater anomaly in the recent freshening of the subpolar North Atlantic. *Journal of Geophysical Research: Oceans, 124*(5), 3333–3360. doi:10.1029/2018JC014686

Dussin, R., Barnier, B., & Brodeau, L. (2016). *The making of Drakkar Forcing Set DFS5*. Grenoble, France: LGGE.

Duyck, E., & De Jong, M. F. (2021). Circulation over the South-East Greenland shelf and potential for liquid freshwater export: A drifter study. *Geophysical Research Letters*, *48*, e2020JB020886. doi.:10.1029/2020GL091948

Gillard, L. C., Hu, X., Myers, P. G., & Bamber, J. L. (2016). Meltwater pathways from marine terminating glaciers of the Greenland ice sheet. *Geophysical Research Letters*, *43*(20), 10873-10882. doi:10.1002/2016GL070969

Gou, R., Feucher, C., Pennelly, C., & Myers, P. G. (2021). Seasonal cycle of the coastal west Greenland current system between Cape Farewell and Cape Desolation from a very high-resolution numerical model. *Journal of Geophysical Research: Oceans*, *126*, e2020JC017017. doi.:10.1029/2020JC017017

Hall, M. M., Torres, D. J., & Yashayaev, I. (2013). Absolute velocity along the AR7W section in the Labrador Sea. *Deep Sea Research Part I: Oceanographic Research Papers*, *72*, 72–87. doi:10.1016/j.dsr.2012.11.005

Holliday, N. P., Bersch, M., Berx, B., Chafik, L., Cunningham, S., & Florindo-López, C., et al. (2020). Ocean circulation causes the largest freshening event for 120 years in eastern subpolar North Atlantic. *Nature communications*, 11, 585. doi: 10.1038/s41467-020-14474-y.

Hu, X., Sun, J., Chan, T.O., & Myers, P. G. (2018). Thermodynamic and Dynamic Ice Thickness Contributions in the Canadian Arctic Archipelago in NEMO-LIM2 Numerical Simulations. *The Cryosphere*, *12*(4), 1233-1247. doi:10.5194/tc-12-1233-2018

Jackson, L. C., Peterson, K. A., Roberts, C. D., & Wood, R. A. (2016). Recent slowing of Atlantic overturning circulation as a recovery from earlier strengthening. *Nature Geoscience*, *9*, 518–522. doi:10.1038/ngeo2715

Katsman, C. A., Spall, M. A., & Pickart, R. S. (2004). Boundary current eddies and their role in the restratification of the Labrador Sea. *Journal of Physical Oceanography*, *34*(9), 1967–1983. doi:10.1175/1520-0485(2004)0342.0.CO;2

Le Bras, I. A. A., Straneo, F., Holte, J., & Holliday, N. P. (2018). Seasonality of freshwater in the East Greenland Current system from 2014 to 2016. *Journal of Geophysical Research: Oceans*, *123*(12), 8828–8848. doi:10.1029/2018JC014511

Li. F., Lozier, M. S., Bacon, S., Bower, A. S., Cunningham, S. A., & De Jong M. F., et al. (2021). Subpolar North Atlantic western boundary density anomalies and the Meridional Overturning Circulation. *Nature Communications*, 12(1), 3002. doi : 10.1038/s41467-021-23350-2

Lin, P., Pickart, R. S., Torres, D. J., & Pacini, A. (2018). Evolution of the Freshwater Coastal Current at the Southern Tip of Greenland. *Journal of Physical Oceanography, 48*(9), 2127-2140. doi:10.1175/JPO-D-18-0035.1

Lique, C., Treguier, A. M., Scheinert, M., & Penduff, T. (2009). A model-based study of ice and freshwater transport variability along both sides of Greenland. *Climate Dynamics, 33,* 685–705. doi:10.1007/s00382-008-0510-7

Lozier, M. S., Bacon, S., Bower, A. S., Cunningham, S. A., de Jong, M. F., de Steur, L., et al. (2017). Overturning in the Subpolar North Atlantic Program: A new international ocean observing system. *Bulletin of the American Meteorological Society, 98,* 737–752. doi:10.1175/BAMS-D-16-0057.1

Luo, H., Castelao, R. M., Rennermalm, A. K., Tedesco, M., Bracco, A., Yager, P., et al. (2016). Oceanic transport of surface meltwater from the southern Greenland ice sheet. *Nature Geoscience, 9*(7), 528-532. doi:10.1038/ngeo2708

Madec, G (2008). *Nemo ocean engine, Note du Pôle de modélisation, 27*. France: Institut Pierre-Simon Laplace (IPSL).

Mortensen, J. (2018). *Report on hydrographic conditions off Southwest Greenland June/July 2017*. NAFO SCR Doc 18/005, Serial No. N6782.

Majumder, S., Castelao, R. M., & Amos, C. M. (2021). Freshwater variability and transport in the Labrador Sea from in situ and satellite observations. *Journal of Geophysical Research: Oceans, 126,* e2020JC016751. doi:10.1029/2020JC016751

Myers, P. G., Castro de la Guardia, L., Fu, C., Gillard, L. C., Grivault, N., Hu, X., et al. (2021). Extreme high Greenland Blocking Index leads to the reversal of Davis and Nares Strait net transport toward the Arctic Ocean. *Geophysical Research Letters, 48,* e2021GL094178. doi:10.1029/2021GL094178

Myers, P. G., Donnelly, C., & Ribergaard, M. H. (2009). Structure and variability of the West Greenland Current in summer derived from 6 repeat standard sections. *Progress in Oceanography, 80*(1–2), 93–112. doi:10.1016/j.pocean.2008.12.003

Myers, P. G., Kulan, N., & Ribergaard, M. H. (2007). Irminger Water variability in the West Greenland Current. *Geophysical Research Letters, 34*(17), 217-239. doi:10.1029/2007GL030419

Nghiem, S. V., Hall, D. K., Mote, T. L., Tedesco, M., Albert, M. R., & Keegan, K., et al. (2012). The extreme melt across the Greenland ice sheet in 2012. *Geophysical Research Letters, 39,* L20502. doi:10.1029/2012GL053611

Pacini, A., & Pickart, R. S. (2021). Meanders of the West Greenland Current near Cape Farewell. *Deep Sea Research Part I: Oceanographic Research Papers,* 179, 103664. doi:10.1016/j.dsr.2021.103664

Pacini, A., Pickart, R.S., Bahr, F., Torres, D.J., Ramsey, A.L., & Holte, J. (2020). Mean conditions and seasonality of the West Greenland Boundary Current System near Cape Farewell. *Journal of Physical Oceanography*. 50(10), 2849–2871, doi:10.1175/JPO-D-20-0086.1

Pennelly, C., Hu, X., & Myers, P. G.(2019). Cross-isobath freshwater exchange within the North Atlantic subpolar gyre. *Journal of Geophysical Research: Oceans*, 124, 6831-6853. doi:10.1029/2019JC015144

Pennelly, C. & Myers, P. G. (2020). Introducing LAB60: A 1/60° NEMO 3.6 numerical simulation of the Labrador Sea. *Geoscientific Model Devlopment*. 13, 4959–4975, doi:10.5194/gmd-2020-111

Pennelly, C., & Myers, P. G. (2021). Impact of different atmospheric forcing sets on modeling Labrador Sea Water production. *Journal of Geophysical Research: Oceans, 126*, e2020JC016452. doi:10.1029/2020JC016452

Rykova, T., Straneo, F., & Bower, A. S. (2015). Seasonal and interannual variability of the West Greenland Current System in the Labrador Sea in 1993-2008. *Journal of Geophysical Research: Oceans, 120*(2), 1318-1332. doi:10.1002/2014jc010386

Rysgaard, S., Boone, W., Carlson, D., Sejr, M. K., Bendtsen, J., & Juul-Pedersen, T., et al. (2020). An updated view on water masses on the pan-west Greenland continental shelf and their link to proglacial fjords. *Journal of Geophysical Research: Oceans, 125*, e2019JC015564. doi:10.1029/2019JC015564

Schulze-Chretien, L. M., & Frajka-Williams, E. (2018). Wind-driven transport of fresh shelf water into the upper 30 m of the Labrador Sea. *Ocean Science, 14*(5), 1247-1264. doi:10.5194/os-14-1247-2018

Smith, G. C., Roy, F., Mann, P., Dupont, F., Brasnett, B., Lemieux, J.-F., et al. (2014). A new atmospheric dataset for forcing ice-ocean models: Evaluation of reforecasts using the Canadian global deterministic prediction system. *Quarterly Journal of the Royal Meteorological Society, 140*(680), 881–894. doi:10.1002/qj.2194

Stein, M. (2004). Climatic overview of NAFO Subarea 1 1991–2000. *Journal of Northwest Atlantic Fishery Science, 34*, 29–40. doi:10.2960/J.v34.m474

Sutherland, D. A., & Pickart, R. S. (2008). The East Greenland Coastal Current: Structure, variability, and forcing. *Progress in Oceanography, 78* (1), 58-77. doi:10.1016/j.pocean.2007.09.006

Tedesco, M., Fettweis, X., Mote, T., Wahr, J., Alexander, P., Box, J. E., & Wouters, B. (2013). Evidence and analysis of 2012 Greenland records from spaceborne observations, a regional climate model and reanalysis data. *The Cryosphere, 7*, 615–630. doi:10.5194/tc-7-615-2013

Thornalley, D. J. R., Oppo, D. W., Ortega, P., Robson, J. I., Brierley, C. M., & Davis, R., et al. (2018). Anomalously weak Labrador Sea convection and Atlantic overturning during the past 150 years. *Nature, 556*, 227–230. doi:10.1038/s41586-018-0007-4

Whitney, M. M., & Garvine, R. W. (2005). Wind influence on a coastal buoyant outflow, *Journal of Geophysical Research*, 110, C03014. doi:10.1029/2003JC002261

Yashayaev, I., & Loder, J. W. (2017). Further intensification of deep convection in the Labrador Sea in 2016. *Geophysical Research Letters*, 44, 1429–1438. doi:10.1002/2016GL071668.

Zou, S., Lozier, M. S., Li, F., Abernathey, R., & Jackson, L. (2020). Density-compensated overturning in the Labrador Sea. *Nature Geoscience, 13*, 121–126. doi: 10.1038/s41561-019-0517-1